Experimental study of new titanium alloy Ti-6Al-4Fe for biomedical application

Mamoun FELLAH[1,2,*], Mohamed LABAIZ [1], Omar ASSALA[1], Mohammed ABDUL SAMAD [3], Iost ALAIN[4], Nacira SASSANE[5,6]

[1]Laboratory of Metallurgy and Engineering Materials, BADJI Mokhtar-Annaba University, Algeria
[2]Mechanical Engineering [2]Department, ABBES Laghrour- Khenchela University, Algeria
[3]Mechanical Engineering Department, King Fahd University of Petroleum & Minerals, Dhahran - 31261, KSA
[4]Laboratory of Metallurgy, ARTS ET METIERS ParisTech, 8, Boulevard Louis XIV, 59046 Lille Cedex, France,
[5]Welding and NDT research cetre (CSC) B.P 64 CHERAGA, Algeria
[6]Laboratory LM2S, physics department, Badji mokhtar Annaba, Algeria
* Corresponding author: mamoun.fellah@yahoo.fr,

Abstract

Titanium (Ti) and its alloys are used extensively in biomedical applications based on their high specific strength, excellent corrosion and tribological resistance. To overcome the potential V toxicity, V was replaced by Nb and Fe, leading to two new V-free α+ β-type Ti-based alloy, i.e., Ti-6Al-7Nb and Ti-5Al-2.5Fe. The purpose of this study is to evaluate the friction and wear behavior of high-strength titanium based alloy. The Oscillating friction and wear tests have been carried out in ambient air under different conditions of normal applied load and sliding speed, as a counter pairs we used the ball of 100Cr. The surface morphology of the titanium alloys have been characterized by SEM, EDAX, micro hardness, roughness analysis measurements.

Keywords: Tribological behavior, Friction and Wear tests, Biomaterial, titanium alloy. Ti-5Al-2.5Fe.

1. Introduction

Titanium alloys possess attractive properties for biomedical applications where the most important factor is biocompatibility. The Ti–6Al–4V alloy has been successfully applied for biomedical applications **[1].** The effect of heat treatment on microstructure has been well understood for this alloy **[2].** It possesses sufficient strength and ductility for use as human body implants **[3].** Moreover, the good corrosion resistance of this alloy in human body environment is known from in vitro and in vivo studies [4].It is very important to select non-toxic elements for biomedical alloys. Although it is difficult to evaluate different kinds of toxicity of alloying elements **[5],** earlier studies have shown that Nb, Ta, Mo, Zr, and Sn additions to Ti are non-toxic **[6].** It must be noted that the Ti–6Al–4V alloy was originally developed for aerospace applications. Recently, vanadium free Ti alloys such as Ti–6Al–7Nb and Ti–13Nb–13Zr have been developed replacing vanadium in Ti–6Al–4V **[7]** because of the reported toxicity and negative tissue response of vanadium ion in vivo **[8].** Release of vanadium ions by the way of passive dissolution or another process involving wear can cause discoloration of the surrounding tissue or an inflammatory reaction causing pain and even leading to loosening owing to osteolysis **[8].** It has been suggested by Khan et al**. [9]** that Ti–

6Al–7Nb can be a better alternative to Ti–6Al–4V because of its corrosion resistance and resistance to loss of mechanical properties with changes in pH in simulated body fluid environment. **[10-12].**

2. Experimental details

2.1- Materials

The materials used in the present study were Ti–6Al–4V, Ti–6Al–4Nb, Ti–6Al–4Fe and Ti–5Al–2.5Fe (all compositions are in mass %). All the alloys were received in the form of circular pancakes of 3cm diameter. The pancakes were supplied by the **MSMP** *Metallurgical Research Laboratory*, FRANCE. The Ti–6Al–4V was obtained in bare form (3 cm in diameter). The microstructures of the surfaces exposed for tribological testing were also studied using an optical microscope (LEIKA DMLM). The images were later analyzed in an image analysis program (Image-Pro Plus, version 4.1, Media Cybernetics, USA). The microstructures were revealed by etching in 10% HF +5% HNO_3 solutions for 5–10s at room temperature.

2.1.1 Physical Characterization

To characterize the microstructure, the specimens were ground and polished with 0.1 nm diamond paste. After preparing the surfaces by dry grinding and polishing, sintered specimens were thermally etched at 1300°C for 27 min and characterized by scanning electron microscopy (*SEM: JOEL JSM-35C*) using an accelerating voltage of 2-15 kv, to investigate the particle size and morphology. Samples were carbon coated to avoid charging during exposure to the electron beam. Linear intermission electron microscopy was employed to observe the morphology of the starting powders and measure their average grain size. The structural evolution and the phase identification was characterized by X-ray diffractometry (XRD) with Cu-K<α> radiation (<λ>Cu=0.15406 nm) in a (<θ>-<2θ>) Bragg-Brentano geometry.

2.1.2 Micro hardness

The hardness and elastic modulus of studied materials was evaluated from the load-penetration depth curves obtained from a nanoindontation tester (*Zwik ZHV 2.5*) with Berkovich diamond indenter (*B-J87*). The elastic constant E_i=1141 GPa and Poisson ration's ν_i = 0.07 are often used for diamond indenter. Prior to the nanoindentation tests, the surface of the sample was polished and wiped with alcohol and dried thoroughly. In order to take the repeatability into account, the test results were acquired from the average of four indentations.

2.1.3 Tribological Characterizations

Friction and wear tests were conducted using a conventional ball-on-disk type Oscillating tribometer testing machine *(TRIBOtester)* under dry conditions in ambient air and 6 mm track radius in accordance with the ASTMG 99, ISO 7148, and ASTM G 133–95 standards. The tests were carried out under a wide range of applied loads (3, 6 and 10 N respectively), as shown in figure 1 with an alumina ball ($Al_2O_{3)}$ for which the young modulus = 310GPa, $HV_{0.05}$ = 2400 and density of 3.97g/cm^3) as a counterface. α-Al_2O_3 ceramics, prepared by high energy ball milling followed by HIP at 1350 °C by the process described earlier, were cut into disk specimens for different types of tests and polished to a surface roughness (Ra) of $0.55 - 0.75$ nm.

Before each test, the specimens and the balls were rinsed ultrasonically in acetone. After the tribological tests, the worn surfaces of the specimens were observed by an optical and scanning electron microscopy (SEM) respectively. Samples and alumina balls were weighed

before and after the tests, but no much significant difference in the weight was observed. So the following wear rate equation was applied:

$$W = V/F.L \quad \text{.....(Eq 01).}$$

Where *V is* the wear volume (μm^3), *F is* the applied load (N) and *L* is the sliding distance (µm). The wear volume was determined by the integration of the worn track profile obtained by laser and mechanical profilometry with :

$$V = \pi h^2 [R-(h/3)] + [R^2\alpha - l(R/2)\cos(\alpha)] \quad \text{..... (Eq 02).}$$

$$h = R(l-\cos\alpha) \quad \text{.....(Eq 03).}$$

$$\alpha = \arcsin(l/2R) \quad \text{.... .....(Eq 04).}$$

Where l is the width of wear trace (µm), *R is the* ball radius (µm), *h is the d*epth of trace (µm).

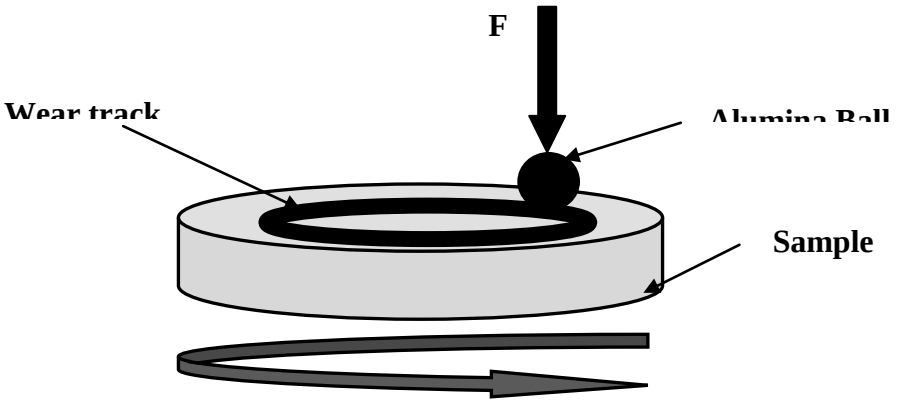

Figure 1: Ball-on-disk configuration used in tribological characterization

3. Results and discussion

3.1 Microstructural analyses, Chemical composition and Mechanical properties

3.1.1- microstructural analyses

The surfaces that were tribological characterized were microstructurally analyzed. In the microstructures that would be presented, beta phase appears dark and the alpha phase light. The microstructures of the alloys are presented in figure 2. All the studied alloys were alpha–beta alloys. Vanadium, niobium and iron are beta stabilizers while aluminium is an alpha stabilizer. Alpha was the dominant phase in all these alloys as evident from the microstructures. The structure of Ti–6Al–4V was fairly fine grained with a grain size of 22.4 µm for primary alpha (Fig. 2). It has also been reported that, owing to a two-phasee quiaxed microstructure, Ti–6Al– 4V is more susceptible to corrosion as the compositional difference across the grain boundaries increases which leads to the galvanic cell formation **[13, 14].**

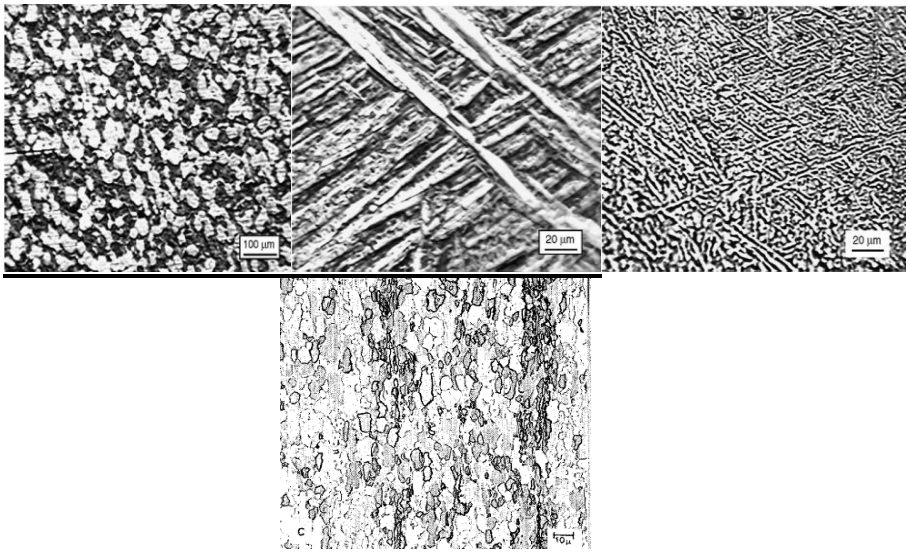

Figure 2: Microstructure of wrought Ti-alloys of the surface of: (a)-Ti–6Al–4V with globular alpha-beta structure, (b) - Optical micrographs of the surface of Ti–6Al–4Nb. (c)-Optical micrographs of the surface of Ti–6Al–4Fe with globular alpha-beta structure and (d) -Ti5Al-2.5Fe with globular alpha-beta structure.

Addition of niobium in Ti-6Al-7Nb increased the grain size considerably as evident from Figure 2 typical Widmanstätten type of structure is observed. Grain boundary alpha can also be seen in the microstructure in a transformed beta matrix. The plate like alpha precipitates that nucleate and grow below the beta transus, produce the Widmanstätten structure [2]. The plates often precipitate in colonies of the same crystallographic orientation as can be noticed in Fig. 2b, because of autocatalytic nucleation [2]. The alpha phase appears to be fine needle shaped (acicular alpha). The Ti–5Al–2.5Fe alloy also possesses a coarse grained structure. Blocky and fine plate like acicular alpha transformed beta (dark) and alpha at prior beta grain boundaries can also be seen in of Ti–5Al–2.5Fe. It has been reported **[15]** that the Ti–5Al–2.5Fe is a near alpha–beta alloy and the alpha phase dominates the properties of this alloy. The volume fraction of beta phase in the alloys is similar as reported in Table 1.

Table 2 shows the chemical composition, while table 3 summarizes the mechanical properties of all titanium alloys used in current study.

Table 1: Image analysis results (grain size and beta fraction).

Materials	Gain size (µm)	Error (µm) +/-	Volume fraction	Error +/-
Ti-6Al-4V	22.4	0.9	0.38	0.02
Ti-6Al-4Nb	826	103	0.39	0.01
Ti-6Al-4Fe	635	100	0.38	0.02
Ti-5Al-2,5Fe	735	100	0.27	0.01

3.1.2- Chemical composition

The standard grade of the Ti-6Al-4V alloy has somewhat higher oxygen content (max. 0.20 % 0,) than the ELI grade (max. 0.13%). The two Ti-6Al-4V alloy grades have a two-phase, globular alpha-beta microstructure (Figure 2b). The few cases of fatigue failure of femoral component stems in wrought Ti-6Al-4V alloy reported in the literature [10] are attributable either to design or to forging faults. The alloy reacts very sensitively to

notches produced by markings (punched letters) in the zone subjected to bending stresses. A good surface finish is a must for each titanium alloy.

Table 2: Chemical composition of wrought titanium alloys for hip joint replacement components in clinical use

Titanium Alloys	C	H_2	N_2	O_2	Fe	Al	V	Nb	Ta	Ti
Ti pure	-	-	-	-	-	-	-	-	-	-
Ti-6Al-4V	0.08	0.015	0.05	0.20	0.30	6.75	4.50	-	-	Basis
Ti-5Al-2-5Fe	0.08	0.015	0.05	0.20	0.30	5.50	-	-	-	Basis
Ti-6Al-7Nb	0.08	0.09	0.05	0.20	0.25	6.50	-	7.50	0.50	Basis

In the Ti-5Al-2.5Fe alloy the alloying element vanadium has been replaced by iron which stabilizes the beta phase**. [16]** This new titanium alloy also exhibits a two-phase, globular alpha-beta microstructure (Fig. 2). It is this two-phase grain structure that is responsible for the high strength values (UTS 862 MPa) of the wrought Ti-5Al-2.5Fe alloy. This alloy is therefore particularly suitable for the manufacture of implants subjected to bending. [**17]**

3.1.3- Mechanical properties.

The mechanical properties were determined on 60 mm long specimens (diameter 4 mm). The mechanical properties of the Ti-6Al-7Nb alloy T 67 in the hot-rolled condition as supplied by the titanium industry and described in the Swiss standard SN 056512; Furthermore, it gives the data of the alloy, supplied as femoral component stems under the trade mark Protasul-100. Young's modulus (110.000 MPa) and the mechanical properties of this new-developed titanium-based alloy Ti-6Al-4Fe- are comparable with those of the clinically proven high- strength Ti-6Al-4V alloy.

Table 3: Mechanical properties of wrouth titanium alloys for hip joint replacement components in clinical use

Composition	Yield strength (Mpa)	UTS (MPa)	Elongation (%)	Reduction area (%)
Ti	485	550	15	25
Ti-6Al-4V	790	860	10	25
Ti-5Al-2,5Fe	895	1020	15	35
Ti-6Al-7Nb	800-1000	900-1100	10-15	25-45

3.1.4 Micro hardness

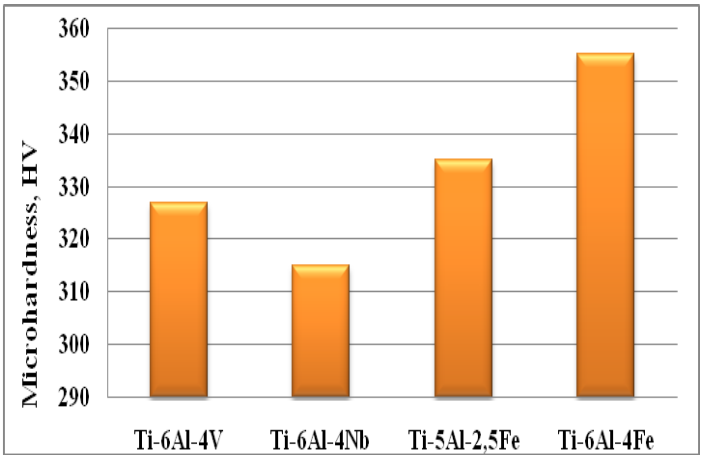

Figure 3: Hardness Vickers values of titanium's alloys.

The load-penetration depth curves obtained from nanoindentation test of different titanium alloys are shown in figure 03. The difference in hardness of the materials is apparent from the difference in the peak depth. Curves illustrate that the micro hardness increased as a function of Fe percentage in titanium alloys. The highest value, 355 HV, was measured in Ti-6Al-4Fe and the lowest value, 315 HV, was obtained for Ti-6Al-7Nb. It is noteworthy to point out that the incursion in the average quantity of iron could also have a partial contribution in the resultant composite hardness.

3.2 Tribological tests

3.2.1- Friction and wear test

After wear tests, the friction coefficient increases rapidly throughout the first meters of sliding and subsequently decreases. After this initial stage, the variations in the curves become smaller and the friction coefficient slightly increases during the remaining testing time. This behavior can be attributed to a polishing process during the wear test, establishing a smooth wear track surface, by ploughing away the surface asperities or roughness irregularities.

As long as the wear test advances, wear tracks become smother and friction coefficients reach a steady state. It should be noted at 3N the samples exhibits much more fluctuations . More fluctuations can be due to extensive roughness of this sample. Additionally, with increasing hardness of the surface by increasing applied loads (Fig. 4) , the actual area of contact decreases; consequently, the COF values decrease.

It is obvious in all experience realized that, the friction coefficient showed a upward trend with the increase of applied loads, and was higher for higher applied load for all the tested samples. As can be seen in figure 4, the average mean values of the COF for samples at a normal load of 2 N is in the range of 0.27-0.4, while it varies between 0.3-0.47 for samples at 4 N, and 0.38-0.49 at 10 N .

It can be observed that with an increase in the normal load, the friction coefficient increases. This is because of an increase in the true contact area upon an increase in the normal load which leads to an increase in the friction coefficient. Figure 05 provides the wear volume of the investigated alloys as a function of the sliding speed. The volumetric wear data reveal that the volume loss, irrespective of alloy composition and microstructure, increases as

the applied load increases. The wear resistance of Ti-5Al-2,5Fe alloy is much lower than that the other materials specially Ti–6Al–4V alloy.

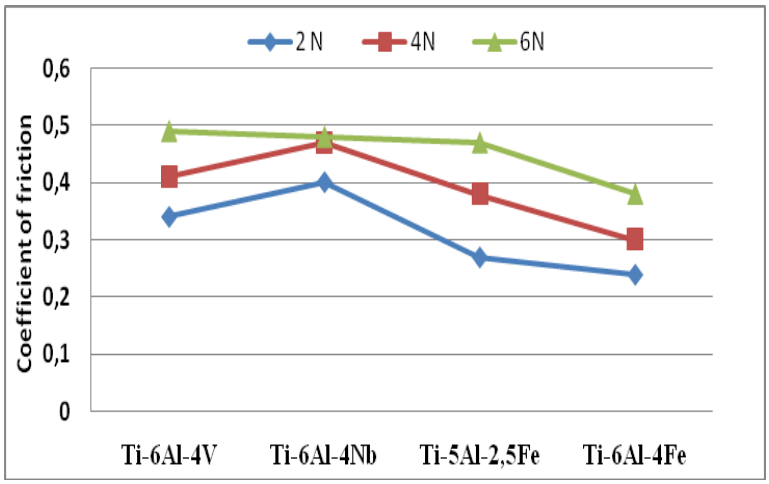

Figure 4: Mean friction coefficien of titanium's alloys under different applied load.

As can be seen from figure 6, the wear loss of Ti-6Al-4V alloy is one order of magnitude higher than that of the Ti-5Al-2,5Fe alloy. This may be expected since the Titanium alloy content the iron irrespective of microstructure, exhibits higher Vickers hardness as compared to Titanium alloy content the Niobium and vanadium.

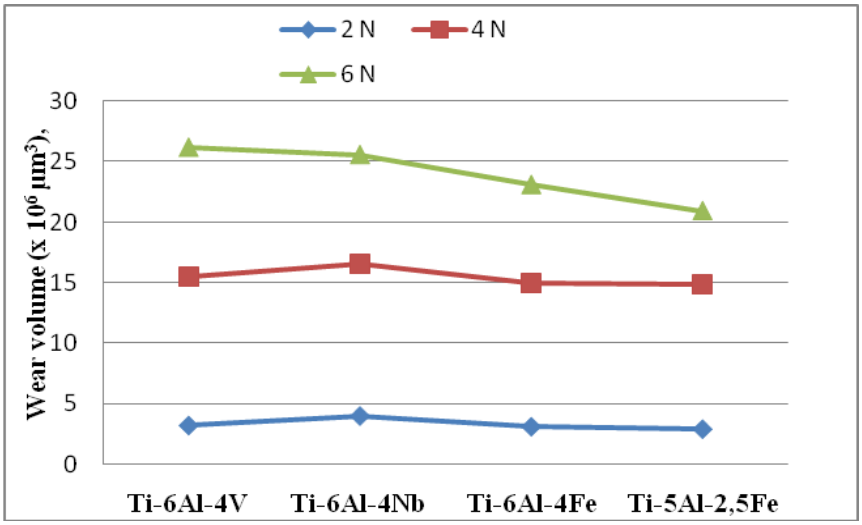

Figure 5: Evolution of Wear volume (x 10^6 µm^3), of titanium's alloys under different applied load.

According to the Archard's law, the volumetric loss of the material is inversely proportional to the hardness value of the material. This implies that the higher the hardness of the material, the smaller is the volume loss. The present alloys exhibit significant difference in hardness values, so that the experimental sliding wear data correlate well with Archard's law.

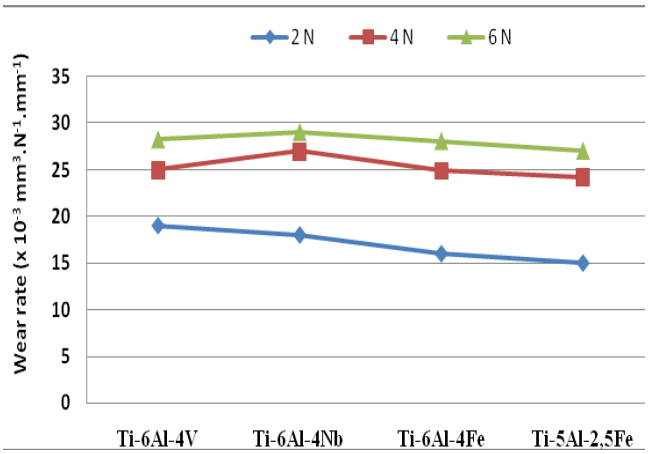

Figure 6: *Evolution of wear rate (x 10^{-3} $mm^3.N^{-1}.mm^{-1}$) of titanium's alloys under different applied load.*

The martensitic microstructure might have enhanced wear resistance due to the higher hardness than that of other microstructures. Thus, the lowest wear loss is obtained for Ti-5Al-2,5Fe alloy having martensitic microstructure and highest hardness among all three investigated materials. The titanium martensites are relatively soft compared to iron-carbon martensites in steel. On the other hand, the grain refinement due to the bcc to hcp transformation and an increase in dislocation density caused by the rapid cooling to form martensite increase the hardness.

The morphological analysis of the wear tracks confirms the above results. The SEM micrographs presented in Fig. 6 show the typical worn surface morphologies of the specimens tested at the lowest and highest applied load. The morphologies of the specimens worn at the intermediate load are not shown because they show intermediate characteristics between these two extremes. On the worn surfaces of both alloys, evidences of abrasion wear can be detected in all tested specimens. Continuous sliding marks with plastically deformed grooves and ridges are seen on the wear tracks independently of the sliding speed. However, the extent of plastic deformation or *''ploughing''* is found to be smaller in the case of the Ti–6Al–4Fe alloy (Figures. 7a–d). Layers with consistent plastic deformations are relatively smooth at all evaluated speeds. Only the shallow wear grooves resulted from the penetrating of hard rigid abrasives and subsequent scratching of the specimen surface by the penetrated abrasives can be observed. The penetration depth depends on the relative hardness of the abrasive with respect to the specimen surface hardness.

As the hardness of the Ti–6Al–4Fe alloy is higher than that of the Ti–6Al-7Nb and Ti-6Al-4V, it is expected that the depth of penetration of the abrasive in the Ti–6Al–4Fe surfaces is less. This results in less material removal from the surface due to ploughing action and smaller extent of plastic flow in the case of Ti–6Al–4Fe. Thus, Ti–6Al–4Fe alloy exhibits significantly less wear rate as compared to the Ti-6Al-4V alloy, it is expected that the depth of penetration of the abrasive in the Ti–6Al–4Fe and Ti–5Al–2.5Fe surface is less. The SEM examination also shows that at least two wear mechanisms are operative in these alloys. Existence of the flakes removed from the contact surface by delamination of material (Figs. 7a, c and e) strongly suggests the occurrence of adhesive wear. During sliding, the contacting

asperities experience an incremental plastic deformation, which accumulates during repeated contacts **[18].**

When a critical value of the accumulated plastic strain is attained; cracks nucleate below the surface and propagate parallel to the surface. As a consequence, flakes of material are detached from the surface by adhesion to the counterpart. Some of transferred material is lost, but some is re-embedded and smeared over the contact surface. In this theory of delamination **[18],** successively discussed and implemented by numerous authors, it is supposed that a critical plastic strain is given by the ductility of the materials. Ti and its alloys are chemically active and have a high ductility, giving rise to the strong tendency to adhesion **[12].**

Therefore, the adhesive strength of the junctions formed is usually much higher than the strength of Ti alloy and such junctions will rupture within the weaker Ti asperities, which accounts for the many craters on the worn surface of Ti alloy. The removal of materials by adhesion is related to large wear loss and it appears that wear rate is determined by the contribution **[12],** successively discussed and implemented by numerous authors, it is supposed that a critical plastic strain is given by the ductility of the materials.

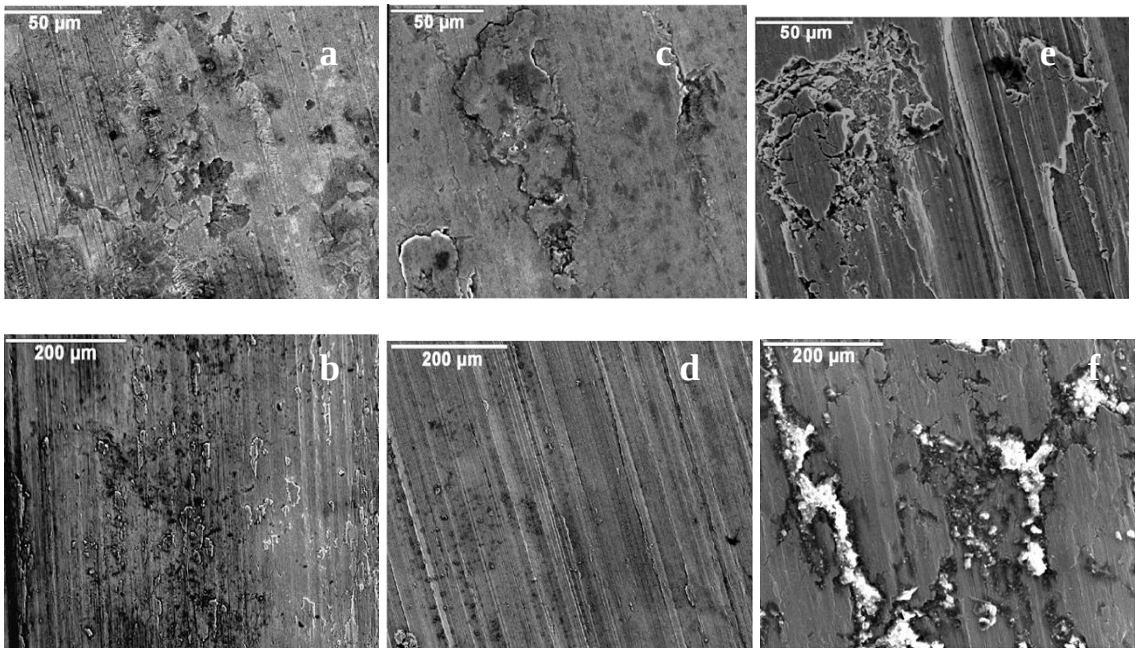

Figure 7: SEM micrographs showing the worn surface of b Ti6Al4V ELI (a and b), Ti-6Al-7Nb (c and d) and Ti–6Al–4Fe *(e and f) specimens tested at sliding speed of 25m/s.*

Ti and its alloys are chemically active and have a high ductility, giving rise to the strong tendency to adhesion **[13].** Therefore, the adhesive strength of the junctions formed is usually much higher than the strength of Ti alloy and such junctions will rupture within the weaker Ti asperities, which accounts for the many craters on the worn surface of Ti alloy. The removal of materials by adhesion is related to large wear loss and it appears that wear rate is determined by the contribution.

4. Conclusion:

In the present study, the friction and wear resistance of Ti–6Al–4V has been compared with that of titanium alloys in which vanadium was replaced with Nb and Fe. It is well known that surface sensitive properties like corrosion and high temperature oxidation are dependent on the chemical composition of the surface. Therefore, the vanadium in Ti–6Al–4V was replaced with the same percentage of Nb and Fe in order to understand the role of chemical composition on the tribological behavior. The Ti–5Al–2.5Fe alloy was evaluated because it has been suggested as a candidate human body implant material.

The friction and wear behaviour of Ti–6Al–4V, Ti–6Al–4Nb, Ti–6Al–4Fe, Ti–5Al–2.5Fe was investigated in simulated body movement and sliding conditions. All materials exhibited good tribological proprieties. The friction of coefficient and wear rate of the alloys, estimated using the ocisilation tribometer. It is obvious in all experience realized that, the friction coefficient showed a upward trend with the increase of applied loads, and was higher for higher applied load for all the tested samples. As can be seen, the average mean values of the COF for samples at a normal load of 2 N is in the range of 0.27-0.4, while it varies between 0.3-0.47 for samples at 4 N, and 0.38-0.49 at 10 N.

5. References

1. H.A. Luckey, F. KubliJr. (Eds.), Titanium Alloys in Surgical Implants (Introduction), ASTM Publication STP 796–800, Philadelphia, 1983, pp. 1–3.

2. FELLAH Mamoun, LABAÏZ Mohamed, ASSALA Omar, DEKHIL Leila, AlAIN Iost, Tribological behavior of biomaterial for total hip prosthesis, Matériaux & Techniques, vol. 102, no 6-7, p. 601 (2014).

3. J.R. Atkinson, B. Jobbins, Properties of engineering materials for use in the body, in: D. Dowson, V. Wright (Eds.), Introduction to the Biomechanics of Joints and Joint Replacement, Mechanical Engineering Publications Ltd., London, 1981.

4. R.J. Solar, Corrosion resistance of titanium surgical implant alloys: a review, in: Corrosion and Degradation of Implant Materials, STP 684, American Society for Testing of Materials, 1979, pp. 259–273.

5. S.G. Steinemann, in: G.D. Winter, J.L. Leray, K. de Groot (Eds.), Corrosion of Surgical Implants—In Vivo and In Vitro Tests, Wiley, 1980, pp. 1–34.

6. Y. Okazaki, Y. Ito, K. Kyo, T. Tateishi, Mater. Sci. Eng. A 213 (1996) 138–147.

7. M. Niinomi, Mechanical properties of biomedical alloys, Mater. Sci. Eng. A 243 (1998) 231–236.

8. J.T. Scales, J. Black, Staining around titanium alloy prosthesis-an orthopaedic enigma, J. Bone Joint Surg. 73B (1991) 534–536.

9. M.A. Khan, R.L. Williams, D.F. Williams, In-vitro corrosion and wear of titanium alloys in the biological environment, Biomaterials 17 (1996) 212–217.

10. FELLAH Mamoun., LABAÏZ Mohamed, ASSALA Omar, ALAIN Iost, Comparative study on tribiological behavior of Ti-6Al-7Nb and SS AISI 316L alloys, for Total hip prothesis, The Minerals, Metals & Materials Society (TMS) Volume 237, P. 237-246. (2014) John Wiley & Sons, Inc. USA. doi: 10.1002/9781118889879. ch32

11. FELLAH Mamoun, LABAÏZ Mohamed, ASSALA Omar, Tribological behavior of Ti-6Al-4V and Ti-6Al-7Nb Alloys for Total Hip Prosthesis, Advances in Tribology, 2014; Article ID 451387, 13 pages, (2014). doi:10.1155/2014/451387.

12. N.P.Suh, Update on the delamination theory of wear, in: D.A. Rigney (Ed.), Fundamentals of Friction and Wear of Materials, ASM, Materials Park, OH, 1980, p.43.

13. H.Dong, T. Bell, Enhanced wear resistance of titanium surfaces by a new thermal oxidation treatment, Wear 238(2000)131137.

14. FELLAH Mamoun, LABAÏZ Mohamed, ASSALA Omar, DEKHIL Leila, AlAIN Iost, Tribological behavior of AISI 316L stainless steel for biomedical applications. Tribology-Materials, Surfaces & Interfaces; 7, no 3: 135-149 (2013).

15. FELLAH Mamoun, LABAÏZ Mohamed, ASSALA Omar, Tribological Behavior of Friction Couple: Metal/Ceramic (Used for Head of Total Hip Replacement). Advances in Bioceramics and Porous Ceramics VI, CESP Volume 34, Issue 6 p. 45-57., John Wiley & Sons, Inc., USA (2013) doi: 10.1002/9781118807811.ch4

16. FELLAH Mamoun, ABDUL SAMAD Mohammed, LABAÏZ Mohamed, ASSALA Omar, Sliding friction and wear performance of the nano-bioceramic α-Al2O3 prepared by high energy milling, Tribology innternational Vol, 91 page 151-159 (2015).

17. ELLAH Mamoun, LABAÏZ Mohamed, ASSALA Omar, DEKHIL Leila, Friction and Wear Behavior of Ti-6Al-7Nb Biomaterial Alloy. Journal of Biomaterial and Nanobiotechnology JBNB, vol. 4, no 04:374. (2013).

18. FELLAH Mamoun, LABAÏZ Mohamed, ASSALA Omar, DEKHIL Leila, Friction and Wear Performance of Titanium Biomaterials, Trends in Biomaterials and Artificial Organs. Vol. 29, no 01(2015).